Desalination and Water Treatment
www.deswater.com
doi: 10.5004/dwt.2020.25097

181 (2020) 399–411
March

Removal of methylene blue dye from synthetic aqueous solutions using dimethylglyoxime modified amberlite IRA-420: kinetic, equilibrium and thermodynamic studies

A.E.M. Mekky[a], M.M. El-Masry[b], R.E. Khalifa[b], A.M. Omer[b], T.M. Tamer[b], Z.A. Khan[c], M. Gouda[d,*], M.S. Mohy Eldin[b,*]

[a]*Chemistry Department, Faculty of Science, Cairo University, Giza, Egypt, email: ataher2211@yahoo.com*
[b]*Polymer Materials Research Department, Advanced Technology and New Materials Research Institute (ATNMRI), City of Scientific Research and Technological Applications (SRTA-City), New Borg El-Arab City 21934, Alexandria, Egypt, Tel. +20 1005318399; emails: mmohyeldin@srtacity.sci.eg (M.S. Mohy Eldin), mansourelmasry@yahoo.com (M.M. El-Masry), randaghonim@yahoo.com (R.E. Khalifa), ahmedomer_81@yahoo.com (A.M. Omer), ttamer85@yahoo.com (T.M. Tamer)*
[c]*Chemistry Department, Faculty of Science, University of Jeddah, Asfan P. O. Box 80203, Jeddah 21589, Saudi Arabia, email: ziyaakhan@gmail.com*
[d]*Chemistry Department, College of Science, King Faisal University, Al-Hassa, Saudi Arabia, email: mgoudaam@kfu.edu.sa*

Received 12 December 2018; Accepted 29 October 2019

ABSTRACT

In this study, methylene blue (MB) dye was removed by adsorption onto dimethyglyoxime modified amberlite IRA-420 (DMG-AMB) beads from aqueous medium. The adsorption data fitted well to kinetic, equilibrium, and thermodynamic models. Equilibrium was reached after only 8 h. The removal percentage increased from around 13.3% to 22.5% with increasing MB concentrations from 2.0 to 8.0 (mg/L), where the adsorbent capacity increased linearly. The analysis of the kinetic data indicated that the adsorption was a second-order process. The Freundlich isotherm model described well the adsorption process. The maximum adsorption capacity, determined from the Langmuir isotherm, was 0.161 mg/g. Moreover, the diffusion mechanism of MB was described by different removal-diffusion models. The film diffusion was found as the rate-limiting process. The pH of the adsorption process was studied; it indicated a determined effect with an exponential increase in the adsorption capacity and removal percentage due to increase in pH from 8.0 to 11.5. A positive impact of the increment in the adsorption temperature was observed for temperature range between 25°C and 60°C. The thermodynamic nature of the process was extracted using Van't Hoff plot. The positive value for the ΔH° (29.69 kJ/mol) indicates the endothermic nature of the process, which explains the increase of the MB cations adsorption efficiency as the temperature increased.

Keywords: Dye removal; MB; Cations–anions exchanger; Amberlite IRA-420; DMG

1. Introduction

A wide range of industries, from textile to plastic, use different types of dyes to colour products, with an estimated amount of dye used and produced. As a result, colour-contaminated wastewater is discharged annually, which causes concern about its effect on the quality of life and the environment [1–5]. A minor concentration of dye in water may be less than 1 ppm, but it can colour the water and turn out to be undesirable [6,7].

* Corresponding authors.

Many individual and merged approaches have been applied in the treatment of wastewater contaminated with coloured materials [8–16]. Adsorption techniques use different adsorbents in the removal of colourant materials [8–10]. Merge of adsorption with other treatment techniques such as precipitation, sonication, and chemical degradation are also used [11–14]. Furthermore, photocatalytic degradation finds application in the treatment of coloured materials [15,16].

MB is a well-recognized dye in the industry, and it has been observed that it causes a wide range of possible health problems [17–19]. Hence, the treatment of MB-coloured wastewater is a requirement, especially since very few treatment techniques are acceptable by the primary industries – paper and textile – that use the dye [20].

The removal capability of a broad spectrum of dyes using different adsorbents nominates the adsorption technique as the one choice for coloured wastewater treatment [21–28]. Synthetic adsorbents such as phosphoric acid doped pyrazole-g-polyglycidyl methacrylate, nano-cross-linked polyacrylonitrile ions exchanger particles, and zinc oxide nanoparticles were investigated [21–23]. Modified natural adsorbents have contributed to the removal of MB-contaminated wastewater [24–28].

In this work, the positive charges of amberlite 420-A anion exchanger have been reversed partially, especially on the surface by treating with dimethylglyoxime (DMG), and applied to remove MB dye from synthetic solution. The operational conditions for MB removal, such as MB concentration, DMG-AMB amount, MB solution pH, adsorption time, and temperature, have been investigated.

Moreover, the kinetics and the isothermal conditions for the removal process have been studied and the obtained results were analyzed.

2. Materials and methods

2.1. Materials

Rohm and Hass supplied Amberlite (IRA 420) ion exchange resin. It is an amine quaternary cross-linked styrene/divinylbenzene copolymer. Table 1 shows a summary of the resin properties [29].

Sodium hydroxide (NaOH), minimum assay 99%, Dimethylglyoxime ($CH_3C(=NOH)C(=NOH)CH_3$), minimum purity ≥97.0%, and Methylene blue, minimum assay 99%, was supplied by Sigma-Aldrich, Germany.

Table 1
Properties of the resin Amberlite IRA-420

Producer	Rohm and Haas
Functionality	$-N^+-(CH_3)_3$
Matrix type	Polystyrene-DVB
Standard ionic form	Cl^-
Total exchange capacity (meq/g)	3.80
Bed porosity	0.32
Wet resin density (g/cm^3)	1.15
Bed density (g/cm^3)	0.68
pH operating range	0–14
Maximum operating temperature	77°C
Mean wet particle radius (mm)	0.30–0.70

2.2. Methods

2.2.1. Preparation of dimethylglyoxime modified Amberlite ions exchanger

The DMG modified Amberlite (DMG-AMB) beads were prepared according to the protocol mentioned in a previous publication [30]. In brief, Amberlite IRA-420 (AMB; 10 grams) was treated by DMG-Sodium hydroxide solution (100 mL; 0.1 N) for 24 h at 60°C under magnetic stirring. Un-reacted DMG and excess of NaOH were washed with hot water before using the DMG modified Amberlite (DMG-AMB) beads.

2.2.2. Methylene blue batch removal experiment

The adsorption experiments were carried out in a batch process by using MB aqueous solution. The MB adsorption studies were performed by mixing 0.1 g of DMG-AMB polymers with 10 mL of MB (10 ppm). The mixture was agitated (100 rpm) at room temperature using magnetic stirrer for 24 h, then left to settle to separate the adsorbent of the liquid phase. The MB concentration (ppm) was measured at the maximum wavelength (λ_{max} = 665 nm) using UV-VIS spectrophotometer and multiplied by 4.0 constant extracted from the slope of the standard curve (Fig. 1).

MB removal percentage is calculated according to the following formula:

$$\text{MB removal}\ (\%) = \left[\frac{(C_0 - C_t)}{C_0}\right] \times 100 \tag{1}$$

where C_0 and C_t (mg L^{-1}) are the initial at zero time and the final concentration of MB at a definite time, respectively.

The removal capacity is calculated according to the following formula:

$$q(\text{mg/g}) = \frac{V(C_0 - C_t)}{M} \tag{2}$$

where q is the uptake capacity (mg/g), V is the volume of the MB ions solution (mL), and M is the mass of the DMG-AMB (g).

2.2.3. Fourier transforms infrared spectroscopic analysis

The Fourier transforms infrared spectroscopic (FTIR) spectra of the Amberlite and DMG-Amberlite were recorded with an FTIR spectrometer in the spectral range 4,000–500 cm^{-1} [30].

2.2.4. Thermal gravimetric analysis

Thermal gravimetric analysis (TGA) of the DMG-AMB and AMB was performed using Thermogravimetric Analyzer (Shimadzu TGA–50, Japan). The measurements were carried out with a heating rate of 20°C/min under a flow of N_2 up to 600°C.

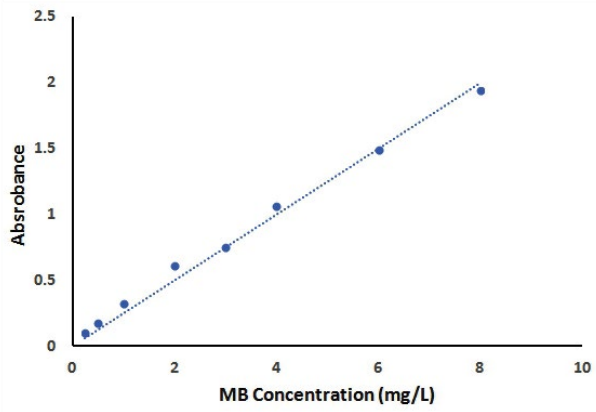

Fig. 1. Standard curve of MB concentrations.

2.2.5. Morphological characterization (SEM) and energy dispersive X-ray analysis

SEM micrographs for the AMB, DMG-AMB and MB-DMG-AMB particles were obtained using Analytical Scanning Electron Microscope (JEOL JSM 6360LA, Japan). The composition (atomic ratios) of the AMB, DMG-AMB and MB-DMG-AMB particles were examined by energy dispersive X-ray (EDAX) combined with scanning electron microscopy.

2.2.6. X-ray diffraction

The crystalline structure of the AMB and DMG-AMB beads were investigated by X-ray diffraction analysis using (Shimadzu 7000) diffractometer.

2.2.7. Reuse ability

The capacity to reuse the DMG-AMB for adsorption of MB ions has been examined by conducting consecutive adsorption–desorption cycles and following the changes in the removal efficiency of MB ions. In the adsorption experiments, DMG-AMB polymer (0.1 g) was agitated (100 rpm) with 20 mL of MB (10 ppm) at room temperature using magnetic stirrer for 6 h. The MB-DMG-AMB particles were regenerated by washing with 20 mL of HCl solution (0.1 N) for 1 h at room temperature, then with distilled water. Finally, the regenerated DMG-AMB particles were removed using NaOH solution (0.1 N) for 1 h at room temperature before being used in the successive adsorption cycle. The process was repeated for 10 cycles.

3. Results and discussion

3.1. Matrix characterization

3.1.1. FTIR analysis

The characteristic bands for the AMB polymeric backbone, poly (styrene-co-divinylbenzene), have been shown in the spectrum at 700; 800; 900; 1,000; 1,400–1,600, and 2,900–3,000 cm^{-1} [31]. The characteristic band for DMG recognized at DMG-AMB shows the peaks at 467 and 904 cm^{-1} which relate to the skeleton deformation vibration of DMG molecules. The peaks at 707 and 980 cm^{-1} are attributed to the (CNO) bending vibration and (NO) stretching vibration modes, respectively. The symmetrical and asymmetrical deformation vibrations of (CH_3) appear at 1,364 and 1,444 cm^{-1}, respectively. The weak peak at 2,930 cm^{-1} is due to the (CH_3) symmetrical stretching vibration (Fig. 2). The relatively broad peak at 3,207 cm^{-1} is attributed to the (OH) stretching vibration. But its lower intensity in comparison with that of the free (OH) group is due to the intramolecular hydrogen bonding, which favours the structural pattern of the DMG molecule itself [32].

3.1.2. Thermal gravimetrical analysis

The modification process of AMB using DMG has been proven by the thermal gravimetric analysis of both AMB and DMG-AMB matrices (Fig. 3). TGA shows a particular "step weight" loss of AMB. Evaporation of physically adsorbed general volatiles in the polymer was noticed up to 270°C where the polymer lost 7% of its weight. The AMB lost some weight (66%) in the second step (270°C–470°C) due to the depolymerization of the polystyrene chains and the degradation of styrene oligomers. In the third step (470°C–600°C), the weight loss (11%) is mostly attributable to divinylbenzene degradation [31–33]. From the figure, the changes of the DMG-AMB thermogram are obvious where a noticeable shift of the thermogram steps has been detected. The first step is continued up to 400°C and lost 42% of its weight. For the second step (400°C–470°C) for DMG-AMB, the weight loss reached 31%. In the final and third steps (470°C–600°C), a 9% weight loss was detected. The changes in the pattern of the first step may be due to the violent decomposition of the DMG moieties which occurred for the temperature range between 140°C and 270°C, resulting in a 90% weight loss [34]. This step overlapped with the first degradation step of AMB (270°C–470°C).

3.1.3. Energy dispersive X-ray analysis

The elemental analysis of the AMB, DMG-AMB and the MB-DMG-AMB particles are presented in Table 2. From the

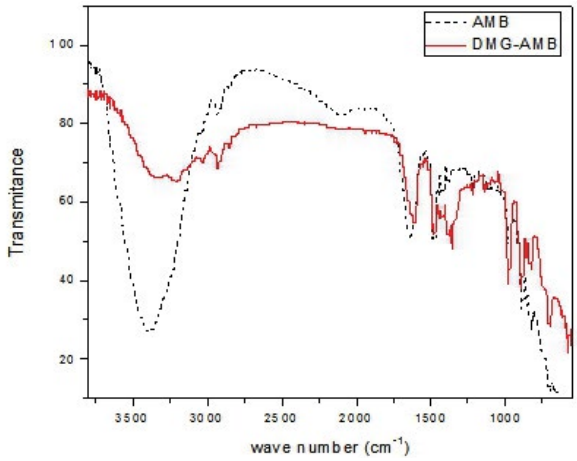

Fig. 2. FTIR spectrum of Amberlite (AMB) and dimethylglyoxime modified Amberlite (DMG-AMB).

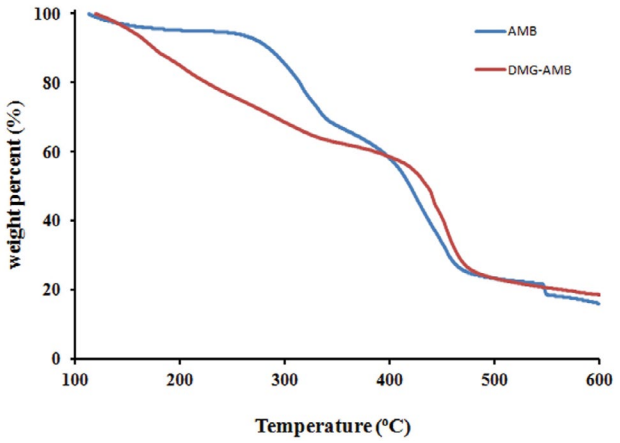

Fig. 3. TGA thermographs of Amberlite (AMB) and dimethylglyoxime modified Amberlite (DMG-AMB).

Table 2
Elemental analysis of C, N, O, and S for the AMB, DMG-AMB, and the MB-DMG-AMB particles

Matrix	C wt%	N wt%	O wt%	S wt%
AMB	38.41	51.44	10.15	NA
DMG-AMB	39.05	31.91	29.05	NA
MB-DMG-AMB	41.71	21.54	36.55	0.20

table, it is clear that changes in the C, N, and O weight percentages due to the modification of the AMB with DMG. The increment of the O weight percentage on the benefits of the N weight percentage is referring to the incorporation of the DMG in the AMB structure. This change is apparent in case of the MB adsorbed on DMG-AMB particles where the appearance of the S further confirms the adsorption process of MB molecules.

3.2. Morphological characterization (SEM)

SEM was used to examine the morphological changes in the surface of the AMB, DMG-AMB, and the MB-DMG-AMB particles and the micrographs are shown in Fig. 4. The surface of AMB particles is a rough shape and two components are observed. One ingredient is flaked, like impeded, in the second component (Fig. 4a). The surface morphology of the DMG-AMB particles (Fig. 4b) became more "smooth" compared with the AMB particles (Fig. 4a) due to the formation of micro-nanometer particles as a coating layer on the surface of the beads. The adsorption of the MB molecules on the surface of the DMG-AMB particles appeared as "aggregates", and the surface turned out to be the roughest one compared with AMB and DMG-AMB beads surfaces (Fig. 4c).

3.2.1. X-ray diffraction analysis

X-ray patterns of AMB and DMG-AMB are shown in Fig. 5. AMB is illustrated as a semi-crystalline structure as a result of a strong interaction between the polystyrene chains through intermolecular hydrogen bonding of positive quaternary groups. A sharp peak at 2θ value 22.22° with 97% crystallinity percentage was observed. A shift of the peak at 2θ to 17.19° and reduction of crystallinity percentage to 50% of DMG-AMB was seen. That observation indicates the incorporation of the DMG into the structure of AMB and increasing the amorphous region by destroying the strong interaction between the polystyrene chains through intermolecular hydrogen bonding of positive quaternary groups.

3.3. Effect of contact time

The impact of variation in contact time on MB removal percentage and removal capacity was investigated, as shown in Fig. 6. It can be seen that the MB removal percentages have been slightly affected by increasing contact time over 8 h. Equilibrium was achieved at a moderately slow rate due to a small number of available adsorption sites. Beyond 8 h of removal time, a slight increase in removal percentages was observed. This behaviour may refer to the reduction of the concentration gradient between the liquid phase and the adsorbent surface [35]. The similar removal behaviour is also observed by Mohy Eldin et al. [36] in a previous publication where MB dye was removed by hydroxamate nano-polyacrylonitrile particles.

On the other hand, the removal capacity shows identical behaviour for the removal percentage which reached 0.207 mg/g at 8 h and slightly increased to 0.2125 mg/g after 16 h (Fig. 6).

3.4. Sorption kinetic models

Three linear kinetic models were used to describe the kinetics of the sorption process selected in this study for describing the MB sorption process using DMG-AMB beads.

The pseudo-first-order kinetic model given by Lagergren and Svenska [37] is as follows:

$$\ln\left(q_e - q_t\right) = \ln q_e - k_1 t \tag{3}$$

The pseudo-second-order rate (chemisorptions) is expressed as [38]:

$$\frac{t}{q_t} = \left(\frac{1}{k_2 q_e^2}\right) + \frac{t}{q_e} \tag{4}$$

The simple Elovich model is represented in the simple form [39]:

$$q_t = \alpha + \beta \ln t \tag{5}$$

q_e and q_t are the amounts of ions adsorbed (mg/g) at equilibrium and time t (min), respectively, k_1 (min^{-1}) is the first-order reaction rate constant, k_2 is the second-order reaction rate equilibrium constant (g/mg min). α represents the initial sorption rate (mg/g min), and β is related to the extent of surface coverage and activation energy for chemisorption (g/mg).

Fig. 7 demonstrates the fitting of the adsorption results using the first-order kinetic model. A good correlation

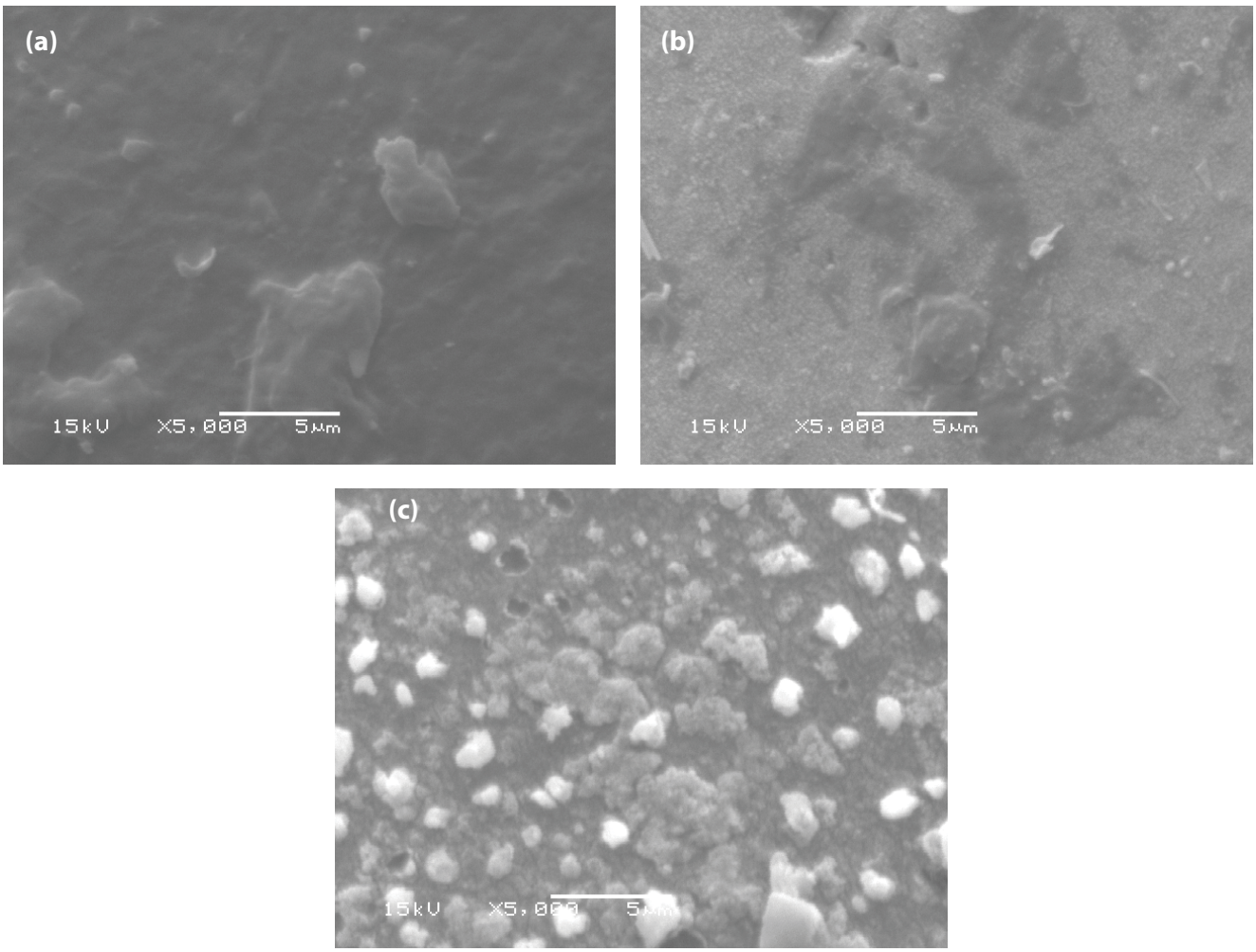

Fig. 4. SEM photographs of: (a) Amberlite (AMB), (b) dimethylglyoxime modified Amberlite (DMG-AMB), and (c) MB-dimethylglyoxime modified Amberlite (MB-DMG-AMB).

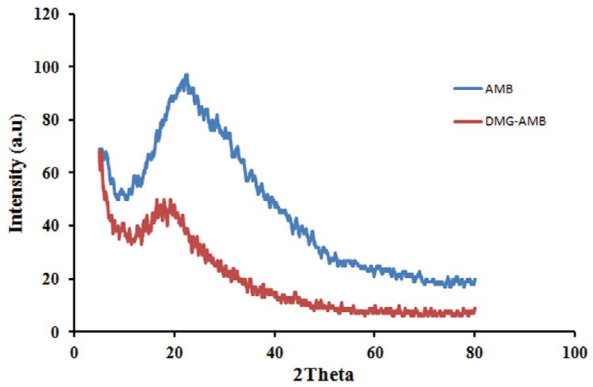

Fig. 5. XRD patterns of: (a) Amberlite (AMB) and (b) dimethylglyoxime modified Amberlite (DMG-AMB).

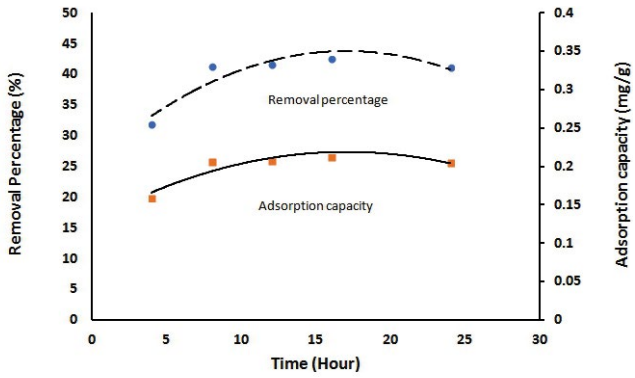

Fig. 6. Effect of adsorption time on MB removal percentage using DMG-Amberlite ions exchanger.

coefficient (R^2; 0.9241) was obtained, and the k_1 calculated value is –0.3458. The comparison of the calculated q_e value (0.183 mg/g) with the experimental one (0.225 mg/g) gives an indication of the unsuitable description of the adsorption process using the first-order kinetic model.

We tried using the pseudo-second-order model to describe the adsorption data (Fig. 8). From the figure, it is evident that the data are fitted very well (R^2; 1). The k_2 and q_e estimated values are 1.7802 and 0.2119 mg/g. Compared with the q_e experimental value (0.225 mg/g), it seems that

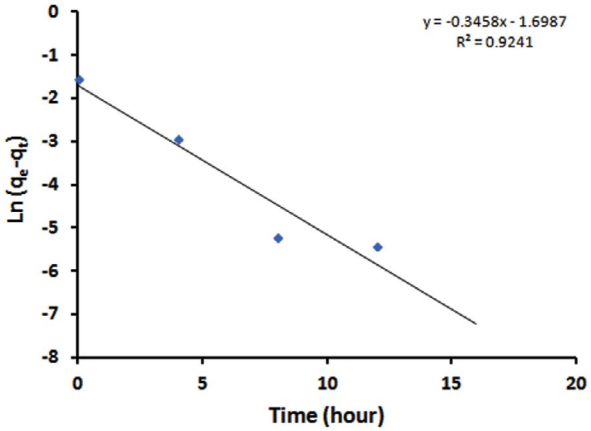

Fig. 7. First order plots for MB removal using DMG-Amberlite ions exchanger.

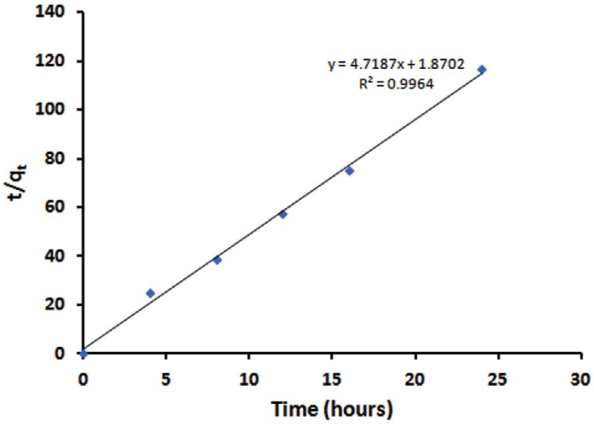

Fig. 8. Second order plots for MB removal using DMG-Amberlite ions exchanger.

the kinetics of the adsorption process is best described by the second-order model. Hence, it has been suggested that the rate-limiting step in these sorption processes may be chemisorptions involving active forces through the sharing or exchanging of electrons between the sorbent and the sorbate [40].

Further investigation of the adsorption process kinetics was performed using the Elovich model and the data are presented in Fig. 9. From the figure, the parameters indicating the number of available sites (β; 0.0259 g/mg) and the removal quantity (α; 0.137 mg/g min) at 1 h can be extracted. These values give an idea about the adsorption process in the early stage [41]. According to the correlation coefficient (R^2; 0.6512), the Elovich model does not describe well the experimental data.

3.5. Sorption mechanisms

We used the diffusion rate equations inside the particulate of Dumwald–Wagner and intraparticle models to calculate the diffusion rate of MB through DMG-AMB beads. For the external mass transfer, we used Boyd model to determine the actual rate-controlling step [42,43].

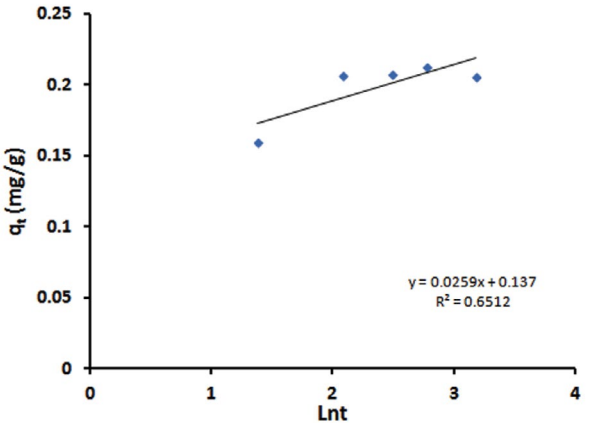

Fig. 9. Simple Elovich plots for MB removal using DMG-Amberlite ions exchanger.

The Dumwald–Wagner model can be expressed as [44]:

$$\log\left(1-F^2\right) = -\left(\frac{K}{2.303}\right)\times t \tag{6}$$

where K is the diffusion rate constant and the removal percentage, and F is calculated by (q_t /q_e). The value of the diffusion rate constant (K) extracted from Fig. 10 is 0.0677 min^{-1}. The poor linear fitting of the adsorption data indicates the non-applicability of Dumwald–Wagner kinetic model.

The intraparticle equation is written as follows [45]:

$$q_t = k_d t^{1/2} + C \tag{7}$$

The adsorption data fitting of MB by DMG-AMB is presented in Fig. 11, where two separate linear portions can be observed and suggest that the removal process consists of surface removal and intraparticle diffusion. The first stage of the adsorption process is presented by the initial linear part of the plot, indicating the effect of the boundary layer, while the second linear portion shows the impact of the intraparticle diffusion [46]. From the intercept and the slope of the second linear portion, the values of the thickness of the boundary layer (C; 0.2089) and the intraparticle diffusion rate (K_d; 0.0001 mg/(g $min^{1/2}$)) are extracted. The larger the intercept, the higher the boundary layer effect [47].

The actual rate-controlling step of the adsorption process was determined by analyzing the data using Boyd et al. [48] model.

$$F = 1-\left(\frac{6}{\pi^2}\right)\exp\left(-B_t\right) \tag{8}$$

where F is the fraction of solute sorbed at different time t and B_t is a mathematical function of F and given by the following equation:

$$F = \frac{q}{q_\alpha} \tag{9}$$

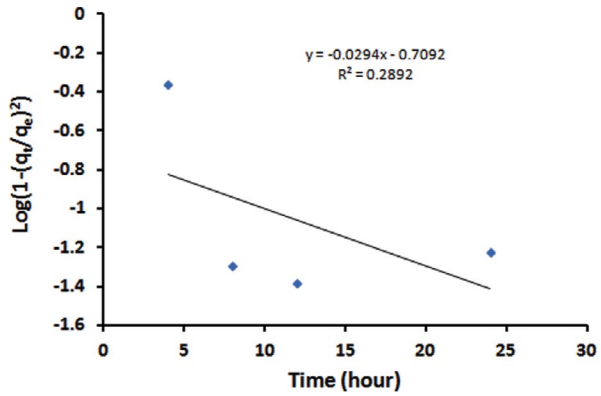

Fig. 10. Dumwald–Wagner plots for intraparticle diffusion of MB removal using DMG-Amberlite ions exchanger.

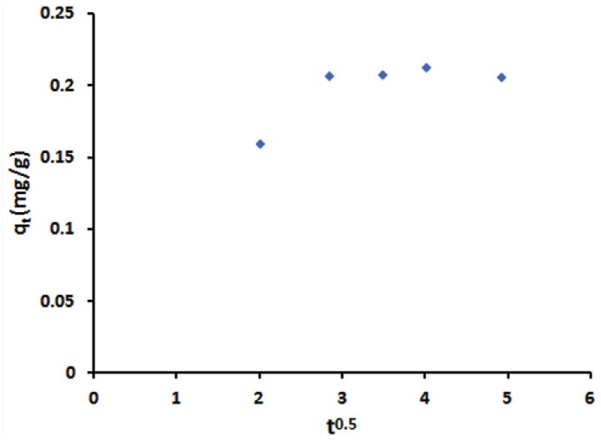

Fig. 11. Intraparticle diffusion plots for MB removal using DMG-Amberlite ions exchanger.

q and q_α represent the amount sorbed (mg/g) at any time t and at infinite time (16 h for the present study). Substituting Eq. (8) into Eq. (9), the kinetic expression becomes:

$$B_t = -0.4978 - \mathrm{Ln}\left(\frac{1-q}{q_\alpha}\right) \tag{10}$$

Fig. 12 shows the plot of B_t vs. t, which is a straight line that does not pass through the origin, indicating that film diffusion governs the rate-limiting process [49]. The methyl hydrophobic groups of DMG play a significant role in changing the hydrophilic–hydrophobic balance of the Amberlite beads. And accordingly, in a way or another, the thickness of the formed liquid boundary layer over the solid surface suggests that the film diffusion is the limiting process [50].

3.6. Effect of MB concentration

Fig. 13 shows the effect of variation of the MB concentration on the removal percentage and the adsorption capacity. The removal percentage increases from 13.3% to 22.5% with an increment of the MB concentration from 2 to 8 ppm.

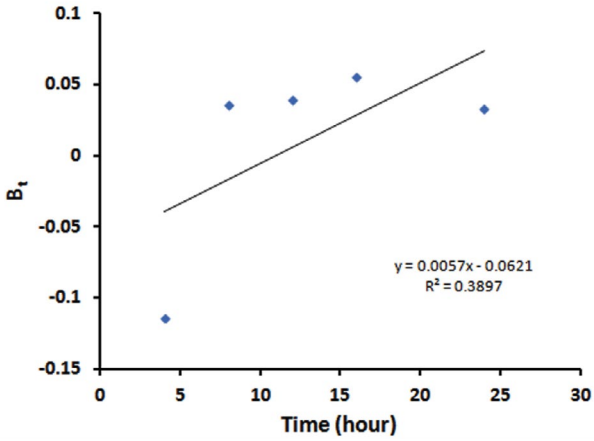

Fig. 12. Boyd expression of the sorption of MB using DMG-Amberlite ions exchanger.

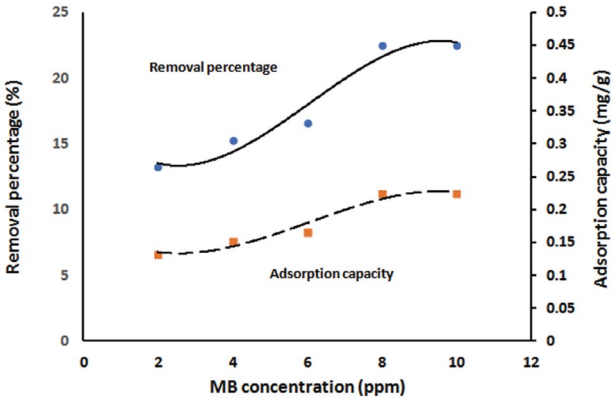

Fig. 13. Effect of MB concentration on the adsorption capacity of DMG-Amberlite ions exchanger.

Further increase in the MB concentration does not affect the removal percentage. On the other hand, the adsorption capacity increased linearly to reach 0.23 mg/g.

3.7. Sorption isotherm models

Different isotherm models describe the adsorption process used. The earliest used one is Freundlich isotherm which postulates that the adsorbent surface has heterogeneous site energies and multi-layers of sorption. On the other hand, the Langmuir isotherm assumes a completely homogeneous surface with a finite identical number of sites, but neglects the interaction between the adsorbed molecules and results in monolayer sorption [51,52].

The linear mathematical formula of the Freundlich model is expressed as follows [53]:

$$\mathrm{Ln}\, q_e = \mathrm{Ln}\, K_F + \frac{1}{n_f}\mathrm{Ln}\, C_e \tag{11}$$

q_e (mg/g) and C_e (mg/L) represent the adsorbent capacity and the adsorbate concentration at equilibrium. The Freundlich

constants, K_F and n_f, represent the adsorption capacity and adsorption intensity.

According to Fig. 14, the Freundlich equation predicts increment of the adsorbed MB amount on the adsorbent, with an increase in the MB concentration in the solution phase, which follows from the obtained results. The high correlation coefficient (R^2 = 0.9919) demonstrates that the adsorption of the MB fully obeyed the Freundlich isotherm. The Freundlich adsorption capacity K_F is 0.0099 (mg/g) while the adsorption intensity n_f is 0.68. The assessed value of n_f < 1, indicating an unfavourable adsorption of the MB by the DMG-AMB beads [54].

On the other hand, the Langmuir isotherm assumes a completely homogeneous surface with a finite number of identical sites and with a negligible interaction between adsorbed molecules which results in monolayer sorption. The linear mathematical formula of the model is presented by the following equation [55]:

$$\frac{C_e}{q_e} = \frac{1}{q_m K} + \frac{C_e}{q_m} \tag{12}$$

q_m is the maximum monolayer adsorption capacity (mg/g) and K is the adsorption energy (L/mg).

Fig. 15 illustrates the Langmuir equation for the MB adsorption by DMG-AMB. According to the R^2 value, which is 0.922, the Langmuir equation represents the sorption process of MB very well. That indicates an excellent mathematical fit. The calculated values of q_m (0.161 mg/g) and K (13.31 L/mg) can be extracted from the figure. An indication of the somewhat low affinity of DMG towards the MB molecules was obtained from the fact that the DMG-AMB was moderately low-efficient for MB removal and had reasonably high energy of sorption (13.31 L/mg).

The dimensionless separation factor (R_L) predicts how favourable or unfavourable the adsorption system is, and is calculated according to the following equation [56]:

$$R_L = \left(\frac{1}{1 + KC_0} \right) \tag{13}$$

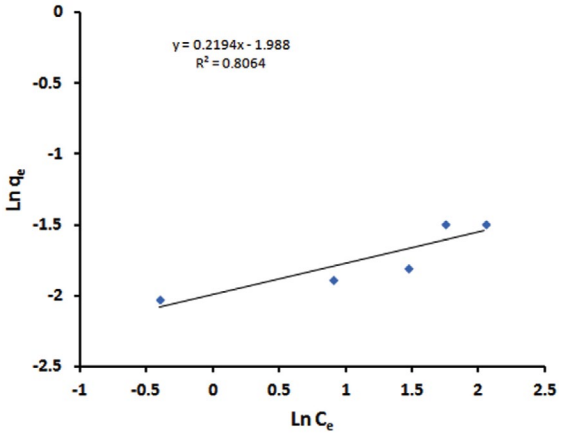

Fig. 14. Freundlich isotherm for MB removal with various initial solution concentrations using DMG-Amberlite ions exchanger.

Table 3 shows favourable adsorption of the MB molecules onto DMG-AMB under the conditions used in this study, since the R_L values ranged between 0.0 and 1.0 [57,58]. This result is in agreement with previously published results by Mohy Eldin et al. [59] of the removal of MB using phosphoric acid-doped pyrazole-g-poly (glycidyl methacrylate) particles.

The Temkin isotherm model is a compromise between the Freundlich and Langmuir isotherm models. It takes into account the impact of indirect adsorbent/adsorbate interactions on the adsorption process, which reduces the heat of adsorption of all molecules in a layer [60] linearly. The linear form can be expressed as follows [61]:

$$q_e = B \,\mathrm{Ln}\, K_T + B \ln C_e \tag{14}$$

K_T is the Temkin maximum binding energy and B is the Temkin constant related to the heat of sorption, which is determined from the slope and the intercept (Fig. 16).

The equilibrium binding constant (K_T) value is 1.72 L/g, corresponding to the maximum binding energy. The constant B (0.12 J/mol) is related to the heat of sorption for DMG-AMB matrix.

The R^2 values obtained from the three equilibrium isotherm models are hereby summarized. The Freundlich isotherm model has the highest R^2 value (0.9919), followed by the Langmuir isotherm model (0.922), and then the Temkin isotherm model with R^2 value of 0.8396. This shows that MB sorption on the polymer is described well by the Freundlich

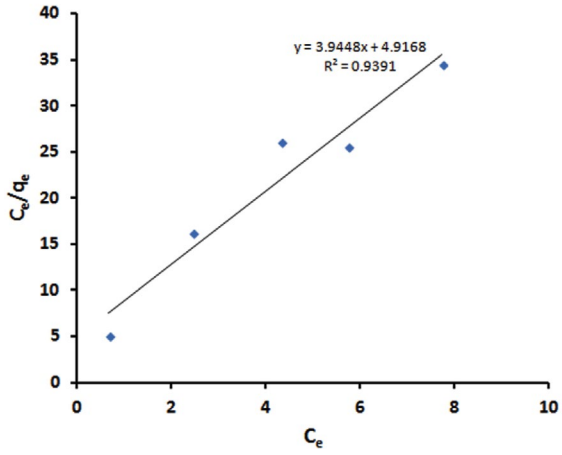

Fig. 15. Langmuir isotherm for MB removal with various initial solution concentrations using DMG-Amberlite ions exchanger.

Table 3
R_L values for different initial MB concentrations

C_0 (mg/L)	R_L
2	0.2863
4	0.167
6	0.1179
8	0.0911
10	0.0742

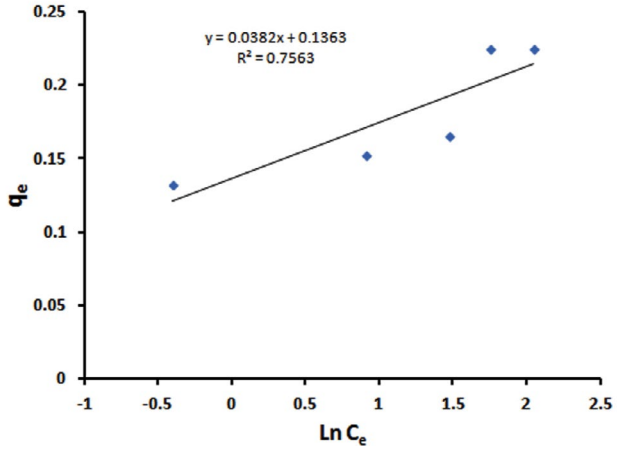

Fig. 16. Temkin isotherm for MB removal with various initial solution concentrations using DMG-Amberlite ions exchanger.

isotherm model, which considers that the adsorbent surface has heterogeneous site energies and multi-layers of sorption.

3.8. Effect of adsorption temperature

Fig. 17 shows the effect of varying the adsorption temperature on the adsorption and thermodynamic parameters. From the figure, it is clear that increasing the adsorption temperature has a positive effect on both the MB removal percentage and the adsorption capacity (Fig. 17a). The MB removal percentage increased from 28% to 58%, while the adsorption capacity increased from 0.142 to 0.290 mg/g. The increment percentage of the adsorption parameters is above 100%. The positive behaviour as a result of increase in the temperature indicates the endothermic nature of the MB adsorption process.

To conclude the spontaneity of the adsorption process, the values of the thermodynamic parameters should be taken into consideration. An automatic system will display a decrease in ΔG° and ΔH° values with increase in the temperature. All the thermodynamic parameters are calculated from the following equations [62,63]:

$$\ln K_0 = \frac{\Delta S}{R} - \frac{\Delta H}{RT} \tag{14}$$

where:

$$K_0 = \frac{q_e}{C_e} \tag{15}$$

$$\Delta G = -RT \ln K_0 \tag{16}$$

where R is the gas constant (8.314 J/mol K), and T is the temperature in K. Table 4 lists the values for the thermodynamic parameters (Fig. 17b). The positive value for the ΔH° (29.69 kJ/mol) indicates the endothermic nature of the process, which explains the increase in the MB cations adsorption efficiency as the temperature increased. The enthalpy change of the chemisorption process (40–120 kJ mol^{-1}) is more significant than the physisorption one [64]. Consequently, the lower value of the heat of adsorption obtained in this study indicates that the adsorption of the MB cations is probably attributable to the physisorption. Conversely, in the kinetics study, it was described that the adsorption is chemisorption. Thus, it is evident from the lower ΔH° value that the physisorption also takes part in the adsorption process. The MB cations adhere to the adsorbent surface only through weak intermolecular interactions. The positive value for the entropy change, ΔS° (67.0366 J/mol K), illustrates the disorderliness at the solid/

Table 4
ΔG° values of the MB cations adsorption on the DMG-AMB under different temperatures

1/T	ΔG°
0.00335	0.1091
0.00319	0.0954
0.00309	0.0789
0.003	0.066

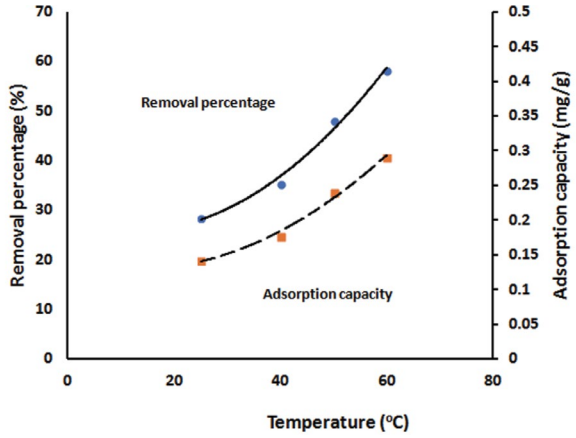

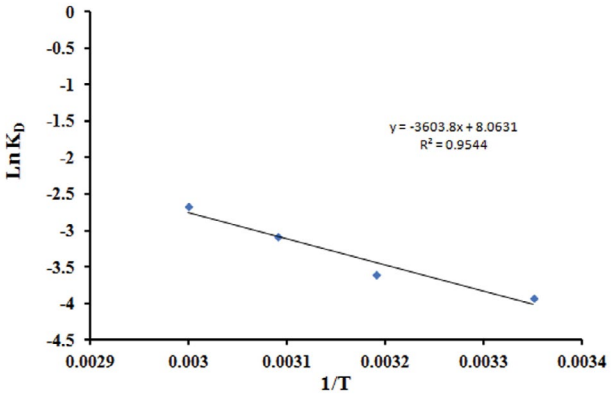

Fig. 17. (a) Effect of adsorption temperature on MB removal percentage using DMG-Amberlite ions exchanger. (b) Van't Hoff plot of the adsorption of MB using DMG-Amberlite ions exchanger.

liquid interface during the adsorption of the MB cations. The ΔG° values reflect the feasibility of the process.

3.9. Effect of adsorption pH

Fig. 18 shows the effect of varying the adsorption pH on the adsorption parameters. Increasing the adsorption pH has a positive impact on both the MB removal percentage and the adsorption capacity. The MB removal percentage increases from 7% to 44%, while the adsorption capacity increases from 0.03652 to 0.220 mg/g. The linear and slow increment is observed for pH range of 1.65 to 8.1, then the rapid exponential increase is detected. The masking effect of the original positive charges over the polymer matrix has reduced as a result of the alkaline medium and enables the negative ones from the DMG be attracted to the positively charged MB molecules.

3.10. Effect of adsorbent amount

Increment of the adsorbent amount has affected a positive effect on the removal percentage and a negative effect on the adsorption capacity, as seen in Fig. 19. The removal percentage increased with increasing adsorbent amount to reach about 90% using 0.5 g of adsorbent. The increment of the available surface for the adsorption process explains the behaviour observed where the removal percentage increased from 37% to 90%. The adsorption capacity decreased from 0.265 to 0.090 mg/g. The fixed amount of the available MB molecules is the limiting factor here.

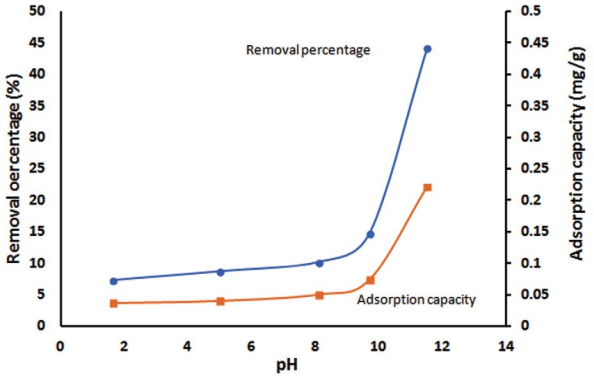

Fig. 18. Effect of adsorption pH on MB removal percentage using DMG-Amberlite ions exchanger.

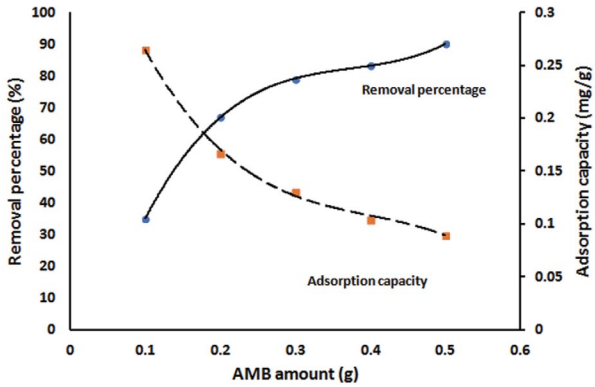

Fig. 19. Effect of adsorbent amount on MB removal percentage using DMG-Amberlite ions exchanger.

3.11. Effect of the agitation speed

The impact of variation in the agitation speed on the adsorption parameters was studied and the obtained data are presented in Table 5. From the table, it is clear that minimal effect was observed with increasing the agitation speed from 100 to 300 rpm. This finding indicates the absence of bulk diffusion, and that the adsorption process was controlled by the diffusion step of the MB molecules inside the pores. This is in agreement with the results given by the kinetic diffusion models (Figs. 10–12).

3.12. Adsorbent affinity

The affinity of the DMG-AMB beads towards MB molecules is measured by the distribution coefficient (K_d), which correlates the amount of the adsorbed MB onto DMG-AMB beads to its concentration in the solution (liquid phase) at equilibrium according to the following relation:

$$K_d = \frac{q_e}{C_e} \tag{17}$$

The K_d values at the variation of both adsorption temperature and pH, as the most determining factors, were calculated and presented in Table 6. From the table, it is clear why both adsorption temperature and pH are the determining factors in the adsorption process. Increasing the adsorption temperature from 25°C to 60°C increased the

Table 5
Effect of the agitation speed on the adsorption parameters

Speed (rpm)	R (%)	Capacity (mg/g)
100	28.43	0.142
150	29	0.145
200	29.4	0.147
250	29.36	0.146
300	29.42	0.147

Table 6
Effect of the adsorption temperature and pH on the distribution coefficient (K_d)

Temperature (°C)	K_d (mL/g)	pH	K_d (mL/g)
25	19.9	1.65	4.0
40	27.3	5	4.4
50	46.3	8.1	5.6
60	69.1	9.7	8.7
		11.5	40.0

K_d value by 3.5 times. More powerful impact is noticed with increasing the adsorption pH from 1.65 to 11.5, where the K_d values increased 10 times.

Table 7 presents a comparative study of the MB removal using different adsorbents in nature. Salisu et al. [65] used alginate graft-polyacrylonitrile beads to remove MB dye. They obtained Langmuir maximum monolayer coverage of 3.51 mg/g. Nature-based adsorbents such as Kenaf *H. cannabinus*-g-PAA and *H. cannabinus*-g-PAA/PAAM show low adsorption capacity (7.0 mg/g) [66] regardless of grafting with functional polymers. Rauf et al. [67] removed MB using gypsum having 36 mg/g adsorption capacity. Patil et al. [68] studied the adsorption of MB in wastewater by low-cost adsorbent rice husk having mg/g adsorption capacity. In this work, low adsorption capacity has been obtained (0.161 mg/g) compared with the cited works in Table 7. Further thorough modification of the AMB is needed to improve its adsorption capacity.

3.13. Reusability

To evaluate the applicability of the DMG-AMB particles in the removal of MB molecules, we tested for 10 successive cycles of adsorption and desorption under selected conditions. The DMG-AMB successfully removed all the MB molecules from the solution after 6 h, keeping its full capacity for the 10 cycles. The obtained results nominate the DMG-AMB particles for practical applications in the removal of MB as a cationic dye model from contaminated water.

4. Conclusion

Dimethylglyoxime modified Amberlite IRA-420 (DMG-AMB) cations exchanger has been prepared and used for the separation of MB. The treatment of Amberlite with DMG has succeeded in converting part of the Amberlite IRA-420 from being an anions exchanger to a cations exchanger. The DMG-AMB successfully removed MB from a synthetic solution. The Langmuir parameter for MB removal (K) indicates that the DMG-AMB was highly efficient for MB removal and had low energy of sorption. The essential characteristics of the Langmuir isotherm (R_L) show favourable removal because the R_L values fall between 0 and 1. The monolayer's adsorption also confirms chemisorption occurs for MB removal. According to Langmuir isotherm, the maximum sorption capacity was found to be 0.161 mg/g. The kinetic data indicated that the sorption was a second-order process.

Table 7
Comparison of the MB adsorption capacity of different adsorbents

Adsorbent matrices	Capacity (mg/g)	References
PAN-g-Alginate	3.51	[65]
Kenaf H. cannabinus-g-PAA	7.11	[66]
Kenaf H. cannabinus-g-PAA/PAAM	7.00	[66]
Gypsum	36	[67]
Rice husk	25	[68]
BMG-AMB	0.161	This work

Moreover, the diffusion mechanism of MB was controlled by the film diffusion process.

The pH of the adsorption process indicated a determining effect with increasing pH from 8.0 to 11.5.

Besides, a positive effect of increasing the adsorption temperature was observed in the range between 25°C and 60°C. The positive value for the ΔH° (29.69 kJ/mol) indicates the endothermic nature of the process, which explains the increase in the MB cations adsorption efficiency as the temperature increased.

The dimethylglyoxime modified Amberlite IRA-420 (DMG-AMB) cations exchanger passed the reusability test, removing all the MB molecules from 10 ppm solution through 10 successive cycles without any loss of efficiency.

In conclusion, to have a higher affinity, we must perform the adsorption process at both a high temperature (between 60°C and 70°C) and in an alkaline medium (pH of 11.0 to 12.0). The modification process induced a little affinity for the cationic molecules. However, the modification of the AMB beads with DMG needs to be investigated more deeply to increase the affinity and the capacity.

References

[1] H. Metivier-Pignon, C. Faur-Brasquet, P.L. Cloirec, Adsorption of dyes onto activated carbon cloths: approach of adsorption mechanisms and coupling of ACC with ultrafiltration to treat coloured wastewaters, Sep. Purif. Technol., 31 (2003) 3–11.
[2] K. Ravi, B. Deebika, K. Balu, Decolourization of aqueous dye solutions by a novel adsorbent: application of statistical designs and surface plots for the optimization and regression analysis, J. Hazard. Mater., B122 (2005) 75–83.
[3] G. McMullan, C. Meehan, A. Conneely, N. Kirby, T. Robinson, P. Nigam, I.M. Banat, R. Marchant, W.F. Smyth, Microbial decolourisation and degradation of textiles dyes, Appl. Microbiol. Biotechnol., 56 (2001) 81–87.
[4] C.I. Pearce, J.R. Lloyd, J.T. Guthrie, The removal of colour from textiles wastewater using whole bacterial cells: a review, Dyes Pigm., 58 (2003) 179–196.
[5] J.W. Lee, S.P. Choi, R. Thiruvenkatachari, W.G. Shim, H. Moon, Evaluation of the performance of adsorption and coagulation processes for the maximum removal of reactive dyes, Dyes Pigm., 69 (2006) 196–203.
[6] T. Robinson, G. McMullan, R. Marchant, P. Nigam, Remediation of dyes in textiles effluent: a critical review on current treatment technologies with a proposed alternative, Bioresour. Technol., 77 (2001) 247–255.
[7] I.M. Banat, P. Nigam, D. Singh, R. Marchant, Microbial decolourization of textile-dye-containing effluents: a review, Bioresour. Technol., 58 (1996) 217–227.
[8] A.K. Jain, V.K. Gupta, A.B. Suhas, Utilization of industrial waste products as adsorbents for the removal of dyes, J. Hazard. Mater., B101 (2003) 31–42.
[9] Y.S. Ho, G. McKay, Sorption of dyes and copper ions onto biosorbents, Process Biochem., 38 (2003) 1047–1061.
[10] J.S. Wu, C.H. Liu, K.H. Chu, S.Y. Suen, Removal of cationic dye methyl violet 2B from water by cation exchange membranes, J. Membr. Sci., 309 (2008) 239–245.
[11] M.X. Zhu, L. Lee, H.H. Wang, Z. Wang, Removal of an anionic dye by adsorption/precipitation processes using alkaline white mud, J. Hazard. Mater., 149 (2007) 735–741.
[12] M. Abbasi, N.R. Asl, Sonochemical degradation of Basic Blue 41 dye assisted by nanoTiO_2 and H_2O_2, J. Hazard. Mater., 153 (2008) 942–947.
[13] J. Garcıa-Montano, L. Perez-Estrada, I. Oller, M.I. Maldonado, F. Torrades, J. Peral, Pilot plant scale reactive dyes degradation by solar photo-Fenton and biological processes, J. Photochem. Photobiol., A, 195 (2008) 205–214.

[14] B. Lodha, S. Chaudhari, Optimization of Fenton-biological treatment scheme for the treatment of aqueous dye solutions, J. Hazard. Mater., 148 (2007) 459–466.
[15] M.R. Sohrabi, M. Ghavami, Photocatalytic degradation of Direct Red 23 dye using UV/TiO_2: effect of operational parameters, J. Hazard. Mater., 153 (2008) 1235–1239.
[16] M. Sleiman, D.L. Vildozo, C. Ferronato, J.M. Chovelon, Photocatalytic degradation of azo dye Metanil Yellow: optimization and kinetic modeling using a chemometric approach, Appl. Catal., B, 77 (2007) 1–11.
[17] D. Ghosh, K.G. Bhattacharyya, Adsorption of methylene blue on kaolinite, Appl. Clay Sci., 20 (2002) 295–300.
[18] I.A.W. Tan, A.L. Ahmad, B.H. Hameed, Adsorption of basic dye on high-surface-area activated carbon prepared from coconut husk: equilibrium, kinetic and thermodynamic studies, J. Hazard. Mater., 154 (2008) 337–346.
[19] I.A.W. Tan, A.L. Ahmad, B.H. Hameed, Adsorption of basic dye using activated carbon prepared from oil palm shell: batch and fixed bed studies, Desalination, 225 (2008) 13–28.
[20] S.M. Ghoreishi, R. Haghighi, Chemical catalytic reaction and biological oxidation for treatment of non-biodegradable textile effluent, .Chem. Eng. J., 95 (2003) 163–169.
[21] M.S. Mohy Eldin, K. Aly, Z.A. Khan, A.E. Meky, T.S. Saleh, A.S. Elbogamy, Development of novel acid-base ions exchanger for basic dye removal: phosphoric acid doped pyrazole-g-polyglycidyl methacrylate, Desal. Wat. Treat., 57 (2016) 24047–24055.
[22] M.S. Mohy Eldin, Y.A. Aggour, M.R. Elaassar, G.E. Beghet, R.R. Atta, Development of nano-crosslinked polyacrylonitrile ions exchanger particles for dyes removal, Desal. Wat. Treat., 57 (2016) 4255–4266.
[23] T.M. Tamer, A.M. Hafez, G.D. Roston, M.S. Mohyeldin, W.M. Abou-Taleb, A. Omer, Formation of zinc oxide nanoparticles using alginate as a template for purification of wastewater, Environ. Nanotechnol. Monitor. Manage., 10 (2018) 112–121.
[24] M.S. Mohy Eldin, M.H. Gouda, M.A. Abu-Saied, Y.M.S. El-Shazly, H.A. Farag, Development of grafted cotton fabrics ions exchanger for dye removal applications: methylene blue model, Desal. Wat. Treat., 57 (2016) 22049–22060.
[25] M.S. Mohy Eldin, M.H. Gouda, M.E. Youssef, Y.M.S. El-Shazly, H.A. Farag, Removal of methylene blue by amidoxime polyacrylonitrile-grafted cotton fabrics: kinetic, equilibrium, and simulation studies, Fibers Polym., 17 (2016) 1884–1897.
[26] R.E. Ghonim, A.M. Omer, T.M. Tamer, W. Salem, M.S. Mohy Eldin, Removal of methylene blue dye from synthetic aqueous solutions using novel phosphonate cellulose acetate membranes: adsorption kinetics, equilibrium, and thermodynamic studies, Desal. Wat. Treat., 144 (2019) 272–285.
[27] C. Liu, A.M. Omer, X.-K. Ouyang, Adsorptive removal of cationic methylene blue dye using carboxymethyl cellulose/k-carrageenan/activated montmorillonite composite beads: isotherm and kinetic studies, Int. J. Biol. Macromol., 106 (2018) 823–833.
[28] A. Shebl, A.M. Omer, T.M. Tamer, Adsorption of cationic dye using novel O-amine functionalized chitosan Schiff base derivatives: isotherm and kinetic studies, Desal. Wat. Treat., 130 (2018) 132–141.
[29] M. Carmona, A. Pérez, A. de Lucas, L. Rodrguez, J.F. Rodriguez, Removal of chloride ions from an industrial polyethyleneimine flocculant shifting it into an adhesive promoter using the anion exchange resin Amberlite IRA-420, React. Function. Polym., 68 (2008) 1218–1224.
[30] Z.A. Khan, A.E.M. Mekky, A.S. Bin Mahfouz, T.S. Saleh, M.S. Mohy Eldin, Separation of nickel (II) ions from synthetic aqueous solutions with novel dimethylglyoxime-modified Amberlite IRA-420: kinetic and equilibrium studies, Desal. Wat. Treat., 81 (2017) 123–133.
[31] L.C.D-S. Maria, M.A.V. Souza, F.R. Santos, L.M.S. Rubenich, M.D.J.F. Ferreira, R.M.P. Sa, Thermogravimetric and Spectrometric Characterizations of Poly(Styrene-co-Divinylbenzene) Containing Phosphinic and Phosphonic Acid Groups, Polym. Eng. Sci., 48 (2008) 1897–1900.
[32] A. Nezamzadeh-Ejhieh, M. Kabiri-Samani, Effective removal of Ni(II) from aqueous solutions by modification of nanoparticles of clinoptilolite with dimethylglyoxime, J. Hazard. Mater., 260 (2013) 339–349.
[33] C.-M. Davidescu, M. Ciopec, A. Negrea, A. Popa, L. Lupa, E.-S. Dragan, R. Ardelean, G. Ilia, S. Iliescu, Synthesis, characterization, and Ni(II) ion sorption properties of poly(styrene-co-divinylbenzene) functionalized with aminophosphonic acid groups, Polym. Bull., 70 (2013) 277–291.
[34] S.M. Pourmortazavi, I. Kohsari, M.B. Teimouri, S.S. Hajimirsadeghi, Thermal behaviour kinetic study of dihydroglyoxime and dichloroglyoxime, Mater. Lett., 61 (2007) 4670–4673.
[35] R. Aravindhan, N.N. Fathima, J.R. Rao, B.U. Nair, Equilibrium and thermodynamic studies on the removal of basic black dye using calcium alginate beads, Colloids Surf., A, 299 (2007) 232–238.
[36] M.S. Mohy Eldin, S.A. El-Sakka, M.M. El-Masry, I.I. Abdel-Gawad, S.S. Garybe, Removal of methylene blue dye from aqueous medium by nano-polyacrylonitrile particles, Desal. Wat. Treat., 44 (2012) 151–160.
[37] S. Langergren, B.K. Svenska, Zur theorie der sogenannten adsorption geloester stoffe, Veternskapsakad Handlingar, 24 (1898) 1–39.
[38] Y.S. Ho, G. McKay, The kinetics of sorption of basic dyes from aqueous solutions by sphagnum moss peat, Can. J. Chem. Eng., 76 (1998) 822–826.
[39] M. Ozacar, I.A. Sengil, A kinetic study of metal complex dye sorption onto pine dust, Proc. Biochem., 40 (2005) 565–572.
[40] Y.S. Ho, G. McKay, Pseudo-second order model for sorption processes, Proc. Biochem., 34 (1999) 451–465.
[41] R.L. Tseng, Mesopore control of high surface area NaOH-activated carbon, J. Colloid Interface Sci., 303 (2006) 494–502.
[42] C. Namasivayam, M.V. Sureshkumar, Removal of chromium (VI) from water and wastewater using surfactant-modified coconut coir pith as a biosorbent, Bioresour. Technol., 99 (2008) 2218–2225.
[43] F.W. Meng. Study on a Mathematical Model in Predicting Breakthrough Curves of Fixed-Bed Removal onto Resin Adsorbent, MS Thesis, Nanjing University, China, 2005, pp. 28–36.
[44] G. McKay, M.S. Otterburn, J.A. Aja, Fuller's earth and fired clay as adsorbents for dyestuffs, Water Air Soil Pollut., 24 (1985) 307–322.
[45] W.J. Weber, J.C. Morris, J. Sanity, Kinetics of Removal on Carbon from Solution, Eng. Div. Am. Soc. Civil Eng., 89 (1963) 31–59.
[46] M. Sarkar, P.K. Acharya, B. Bhaskar, Modeling the removal kinetics of some priority organic pollutants in water from diffusion and activation energy parameters, J. Colloid Interface Sci., 266 (2003) 28–32.
[47] K. Kannan, M.M. Sundaram, Kinetics and mechanism of removal of methylene blue by removal on various carbons: a comparative study, Dye Pigm., 51 (2001) 25–40.
[48] G.E. Boyd, A.W. Adamson, I.S. Myers, The exchange removal of ions from aqueous solutions by organic zeolites; kinetics, J. Am. Chem. Soc., 69 (1947) 2836–2848.
[49] A.E. Ofomaja, Kinetic study and sorption mechanism of methylene blue and methyl violet onto mansonia (*Mansonia altissima*) wood sawdust, Chem. Eng. J., 143 (2008) 85–95.
[50] A. Naghash, A. Nezamzadeh-Ejhieh, Comparison of the efficiency of modified clinoptilolite with HDTMA and HDP surfactants for the removal of phosphate in aqueous solutions, J. Ind. Eng. Chem., 31 (2015) 185–191.
[51] F. Gode, E. Pehlivan, A comparative study of two chelating ion-exchange resins for the removal of chromium(III) from aqueous solution, J. Hazard. Mater. B, 100 (2003) 231–243.
[52] G. Gode, E. Pehlivan, Removal of Cr (III) ions by Turkish brown coals, Fuel Process. Technol., 86 (2005) 875–884.
[53] Y.S. Ho, Effect of pH on lead removal from water using tree fern as the sorbent, Bioresour. Technol., 96 (2005) 1292–1996.
[54] M.M. Dubinin, E.D. Zaverina, L.V. Radushkevich, Sorption, and structure of activated carbons, I. investigation of organic vapor removal, Zh Fiz Khim, 21 (1947) 1351–1362.
[55] N. Unlu, M. Ersoz, Removal characteristics of heavy metal ions onto a low-cost biopolymeric sorbents from aqueous solution, J. Hazard. Mater., 136 (2006) 272–280.
[56] A. Mohammad, A.K.R. Rifaqat, A. Rais, A. Jameel, Removal studies on *Citrus reticulata* (fruit peel of orange): removal and

recovery of Ni(II) from electroplating wastewater, J. Hazard. Mater., 79 (2000) 117–131.
[57] Y.S. Ho, J.F. Porter, G. McKay, Equilibrium isotherm studies for the sorption of divalent metal ions onto peat: copper, nickel and lead single component systems, Water Air Soil Pollut., 141 (2002) 1–33.
[58] I.A.W. Tan, A.L. Ahmad, B.H. Hameed, Removal of basic dye using activated carbon prepared from oil palm shell: batch and fixed bed studies, Desalination, 225 (2008) 13–28.
[59] M.S. Mohy Eldin, K.M. Aly, Z.A. Khan, A.E.M. Mekky, T.S. Saleh, A.S. Al- Bogami, Removal of methylene blue from synthetic aqueous solutions with novel phosphoric acid-doped pyrazole-g-poly(glycidyl methacrylate) particles: kinetic and equilibrium studies, Desal. Wat. Treat., 57 (2016) 27243–27258.
[60] B.H. Hameeda, L.H. China, S. Rangarajan, Removal of 4-chlorophenol onto activated carbon prepared from rattan sawdust, Desalination, 225 (2008) 185–198.
[61] M.I. Temkin, V. Pyzhev, Kinetics of ammonia synthesis on promoted iron catalysts, Acta Physicochim., 12 (1940) 327–356.
[62] T.A. Khan, S. Dahiya, I. Ali, Use of kaolinite as adsorbent: equilibrium, dynamics and thermodynamic studies on the adsorption of Rhodamine B from aqueous solution, Appl. Clay Sci., 69 (2012) 58–66.
[63] G. Zhao, J. Li, X. Wang, Kinetic and thermodynamic study of 1-naphthol adsorption from aqueous solution to sulfonated graphene nanosheets, Chem. Eng. J., 173 (2011) 185–190.
[64] M. Alkan, O. Demirbas, S.Ç.M. Dogan, Sorption of acid red 57 from aqueous solution onto sepiolite, J. Hazard. Mater., B116 (2004) 135–145.
[65] A. Salisu, M.M. Sanagia, A. Abu Naim, K.J. Karim, Removal of methylene blue dye from aqueous solution using alginate grafted polyacrylonitrile beads, Der Pharma Chemica, 7 (2015) 237–242.
[66] G. Sharma, M. Naushad, D. Pathania, A. Mittal, G.E. El-desoky, Modification of Hibiscus cannabinus fiber by graft copolymerization: application for dye removal, Desal. Wat. Treat., 54 (2015) 3114–3121.
[67] M.A. Rauf, I. Shehadeh, A. Ahmed, A. Al-Zamly, Removal of methylene blue from aqueous solution by using gypsum as a low cost adsorbent, Int. J. Chem. Mol. Nucl. Metall. Eng., 3 (2009) 369–374.
[68] M.A. Patil, J.K. Shinde, A.L. Jadhav, S.R. Deshpande, Adsorption of Methylene Blue in waste water by low cost adsorbent Rice husk, Int. J. Eng. Res. Technol., 10 (2017) 246–252.